Supplementary Information

Title: Composition-Directed $Fe_xMo_{2-x}P$ Bimetallic Catalysts for Hydrodeoxygenation Reactions

Author(s): Dallas J. Rensel,[a†] Jongsik Kim,[a†] Varsha Jain,[b†] Yolanda Bonita,[a] Neeraj Rai,[b*] and Jason C. Hicks[a*]

[a] Department of Chemical and Biomolecular Engineering, 182 Fitzpatrick Hall, University of Notre Dame, Indiana 46556, United States

[b] Dave C. Swalm School of Chemical Engineering and Center for Advanced Vehicular Systems, Mississippi State University, Mississippi 39762, United States

[†] Authors DJR, JK, and VJ contributed equally.

Table of Contents

The 2nd reaction mechanism (HDO2)

After adsorption of C_6H_5OH on the catalyst surface (Fig. S7 (a) and S8 (a); Eqn. (S1)), the $C_6H_5OH^*$ is subsequently dissociated to produce phenyl ($C_6H_5^*$) and hydroxyl species (OH*) adsorbed on the surface (Fig. S7 (b)-(c) and S8 (b)-(c); Eqn. (S2)). Notably, this step exhibits activation energy barriers of 0.53 eV for Fe_1Mo_1P and 0.94 eV for $Fe_{1.5}Mo_{0.5}P$. This provides evidence that $C_{AROMATIC}$-O bond scission is energetically more favorable on Fe_1Mo_1P rather than $Fe_{1.5}Mo_{0.5}P$, which can result mainly from greater partial charge on metallic species for the Fe_1Mo_1P surface (*i.e.*, +0.81 |e|) compared to the $Fe_{1.5}Mo_{0.5}P$ surface (*i.e.*, +0.63 |e|). Following dissociative adsorption of H_2 species on the surface (H*, Fig. S7 (d) and S8 (d); Eqn. (S3)), rotation of $C_6H_5^*$ species in the presence of H* takes place (Fig. S7 (e) and S8 (e); Eqn. (S4)). The activation energy barriers for $C_6H_5^*$ rotation are 0.15 eV and 0.27 eV for Fe_1Mo_1P and $Fe_{1.5}Mo_{0.5}P$ respectively, which correlates with the stronger adsorption of C_6H_5OH on the surface of $Fe_{1.5}Mo_{0.5}P$ than Fe_1Mo_1P, as discussed in the main manuscript. H transfer to $C_6H_5^*$ species subsequently occurs to form C_6H_5-H* species (Fig. S7 (f) and S8 (f); Eqn. (S4)), showing activation energy barriers of 0.39 eV for Fe_1Mo_1P and 0.41 eV for $Fe_{1.5}Mo_{0.5}P$. After adsorbing benzene species ($C_6H_6^*$) with adsorption energies of -1.7 eV for Fe_1Mo_1P and -2.28 eV for $Fe_{1.5}Mo_{0.5}P$ (Fig. S7 (g) and S8 (g)), the surfaces desorb C_6H_6 species (Eqn. (S7)) with desorption energies of 1.01 eV and 1.52 eV for Fe_1Mo_1P and $Fe_{1.5}Mo_{0.5}P$, respectively. Formation of H_2O species and their subsequent desorption from the surfaces also occurs (Eqn. (S5) and (S6)), while activation energy barriers required to form H_2O are 0.69 eV and 1.02 eV for Fe_1Mo_1P and $Fe_{1.5}Mo_{0.5}P$ respectively. Importantly, $C_{AROMATIC}$-O bond cleavage of $C_6H_5OH^*$ requires the largest energy barriers among three major endothermic elementary steps stated above and therefore can be considered as the slowest, rate-determining step in HDO2.

$$C_6H_5OH\,(g) + * \leftrightarrow C_6H_5OH^* \quad (S1)$$

$$C_6H_5OH^* + * \leftrightarrow C_6H_5^* + OH^* \quad (S2)$$

$$H_2\,(g) + 2^* \leftrightarrow 2H^* \quad (S3)$$

$$C_6H_5^* + H^* \xleftrightarrow{C_6H_5^*\ rotation} C_6H_6^* + {}^* \quad (S4)$$

$$H^* + OH^* \leftrightarrow H_2O^* + {}^* \quad (S5)$$

$$H_2O^* \leftrightarrow H_2O\,(g) + {}^* \quad (S6)$$

$$C_6H_6^* \leftrightarrow C_6H_6\,(g) + {}^* \quad (S7)$$

The 3rd reaction mechanism (HDO3)

The 3rd mechanism postulates that the C atom vicinal to the O atom in $C_6H_5OH^*$ can act as a nucleophilic site to attract H*. Interestingly, rather than forming a reaction intermediate where H is bound to the aromatic C atom, it was energetically more favorable to form a reaction intermediate C_6H_5-OH_2* where the H atom is connected to OH (Fig. S9 (a)-(c) and S10 (a)-(c); Eqn. (S8)-(S10)), thereby modifying the series of elementary steps, accordingly. As shown in Fig. S9 (d)-(e), S10 (d)-(e), rotation of OH renders H atom of C_6H_5-OH_2* to back-attack C_6H_5 species, resulting in the generation of C_6H_5-H* without involving the ring rotation step found on both HDO1 and HDO2 (Eqn. (S11)-(S12)). This step requires the largest activation barriers of 1.07 eV for Fe_1Mo_1P and 1.68 eV for $Fe_{1.5}Mo_{0.5}P$ throughout all elementary steps. Although this reaction mechanism also supports experimental observation that Fe_1Mo_1P with the greater surface Lewis acid character can facilitate the phenol HDO in comparison with Fe-rich analogue, this mechanism is unlikely due to higher activation energy barriers than alternative pathways (*i.e.*, HDO1 and HDO2).

$$C_6H_5OH\,(g) + * \leftrightarrow C_6H_5OH^* \quad (S8)$$

$$H_2\,(g) + 2^* \leftrightarrow 2H^* \quad (S9)$$

$$C_6H_5OH^* + H^* \leftrightarrow C_6H_5 - OH_2^* + * \quad (S10)$$

$$C_6H_5 - OH_2^* + * \overset{Hydroxyl\ rotation}{\leftrightarrow} C_6H_5 - OH_2^* + * \quad (S11)$$

$$C_6H_5 - OH_2^* + * \leftrightarrow C_6H_6^* + OH^* \quad (S12)$$

$$H^* + OH^* \leftrightarrow H_2O^* + {}^* \quad (S13)$$

$$H_2O^* \leftrightarrow H_2O\,(g) + {}^* \quad (S14)$$

$$C_6H_6^* \leftrightarrow C_6H_6\,(g) + {}^* \quad (S15)$$

Table S1 Cell parameters of Fe_1Mo_1P and $Fe_{1.5}Mo_{0.5}P$ computed using 2 X 4 X 2 supercell via PW91.

cell parameter (Å)	Fe_1Mo_1P		$Fe_{1.5}Mo_{0.5}P$	
	experimental	computed	experimental	computed
a	11.84	11.75	11.76	11.78
b	14.60	14.80	14.44	14.11
c	13.56	13.48	13.40	13.35

Table S2 Surface energies for Fe_1Mo_1P and $Fe_{1.5}Mo_{0.5}P$.

facet	Fe_1Mo_1P (eV $\dot{A}^{-2}$)	$Fe_{1.5}Mo_{0.5}P$ (eV $\dot{A}^{-2}$)
(100)	0.18	0.13
(010)	0.17	0.15
(001)	0.16	0.16
(211)	0.08	0.07
(112)	0.01	0.01

Table S3 Molar ratios of Fe to Mo for $Fe_xMo_{2-x}P$ materials.

target	bulk [a]	(near) surface [b]
0.79	0.79 (± 0.07)	0.80 (± 0.03)
1	0.98 (± 0.08)	1.06 (± 0.05) [c]
1.30	1.33 (± 0.11)	1.17 (± 0.09)
1.67	1.70 (± 0.13)	1.81 (± 0.07)
3	3.44 (± 0.11)	2.78 (± 0.06)

[a] via ICP-OES. [b] via XP spectra. [c] 1.06 (± 0.15) via EDX.

Table S4 *In situ* DRIFT bands of pyridine adsorbed on Lewis or Brønsted acid sites present in $Fe_{0.99}Mo_{1.01}P$.

	band [a] (cm^{-1})	
	ν_{19a}	ν_{19b}
Lewis acid sites	1490-1500	1445-1460
Brønsted acid sites	1490-1500	1510-1560

[a] See Fig. S3.

Table S5 Bond lengths for Fe_1Mo_1P and $Fe_{1.5}Mo_{0.5}P$.

bond [a]	Fe_1Mo_1P (Å)	$Fe_{1.5}Mo_{0.5}P$ (Å)
C-Fe	2.13	2.40
O-Fe	2.10	2.30
O-Mo_1	3.16	2.82
O-Mo_2	3.12	-
O-P	2.40	3.86
H-Fe	2.52	3.24
H-Mo	2.94	3.34
H-P	1.75	4.40

[a] See atoms given in Fig. S11.

Table S6 Effect of altering the K-points grid on activation energy barrier for Fe_1Mo_1P and $Fe_{1.5}Mo_{0.5}P$.

parameter	Fe_1Mo_1P		$Fe_{1.5}Mo_{0.5}P$	
	2 X 2 X 1 grid	gamma point	2 X 2 X 1 grid	gamma point
activation energy barier (eV) for C-O cleavage [a]	0.390	0.391	0.772	0.773

[a] computed on (112) facet.

Table S7 Adsorption energies of *n*-alkane homologues on the (112) facets for Fe_1Mo_1P and $Fe_{1.5}Mo_{0.5}P$.

n-alkane	Fe_1Mo_1P (eV)	$Fe_{1.5}Mo_{0.5}P$ (eV)
C_2H_6	-0.20	-0.17
C_3H_8	-0.24	-0.19
C_4H_{10}	-0.22	-0.17
C_5H_{12}	-0.23	-0.19
C_6H_{14}	-0.20	-0.15
C_7H_{16}	-0.23	-0.19

Table S8 Activation energies required in rate-determining steps on $Fe_XMo_{2-X}P$ materials under different reaction pathways.

	HDO1	HDO2	HDO3
Fe_1Mo_1P	0.39 eV	0.53 eV	1.07 eV
$Fe_{1.5}Mo_{0.5}P$	0.77 eV	0.94 eV	1.68 eV

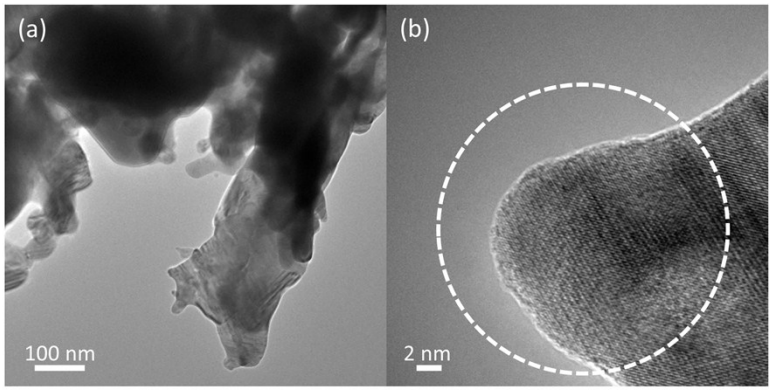

Fig. S1 HRTEM images of $Fe_{0.99}Mo_{1.01}P$. White, dotted circle in (b) indicates a spot used for surface compositional analysis via EDX.

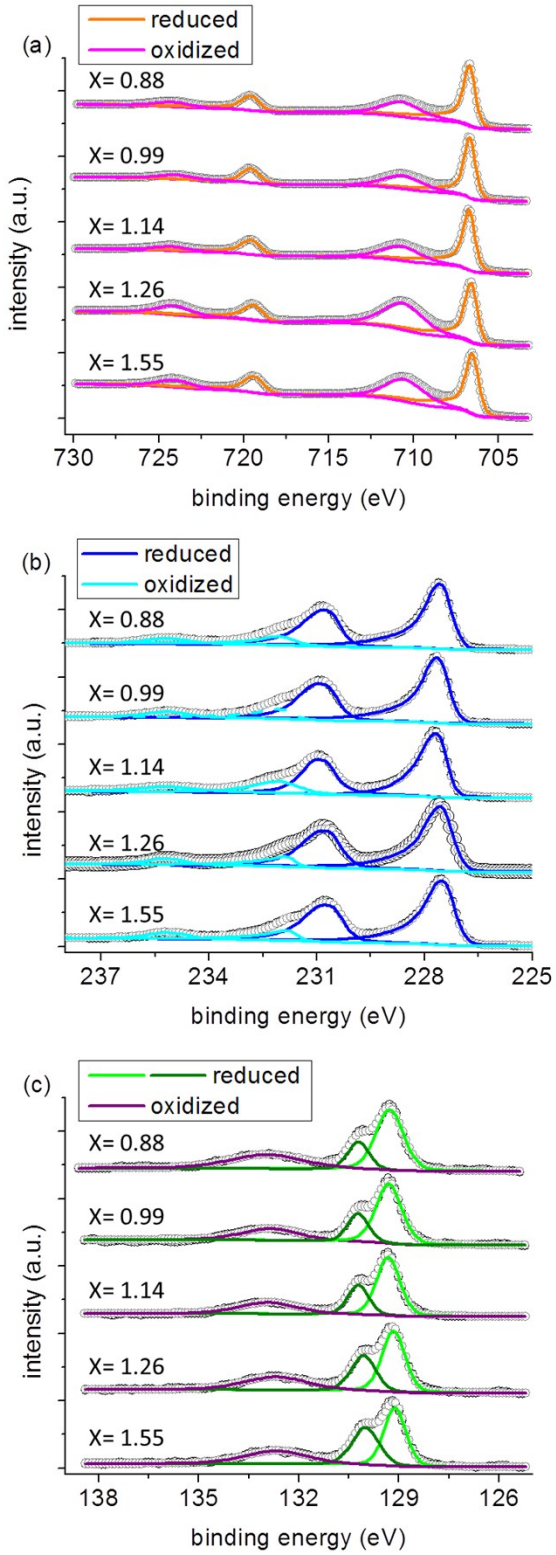

Fig. S2 XP spectra of $Fe_XMo_{2-X}P$-catalysts: (a) Fe 2p, (b) Mo 3d, and (c) P 2p regions. Empty circles and solid lines indicate raw and fitted data, respectively.

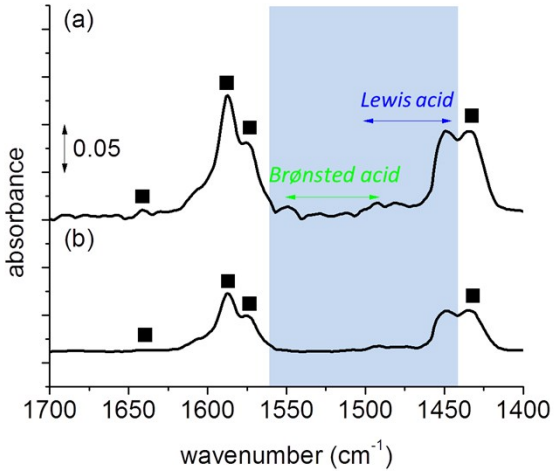

Fig S3 *In situ* DRIFT spectra (background subtracted) of $Fe_{0.99}Mo_{1.01}P$ materials after their exposure to pyridine at 150 °C: (a) $Fe_{0.99}Mo_{1.01}P$ reduced at 650 °C and (b) $Fe_{0.99}Mo_{1.01}P$ reduced at 850 °C. Black square indicates the gaseous pyridine.

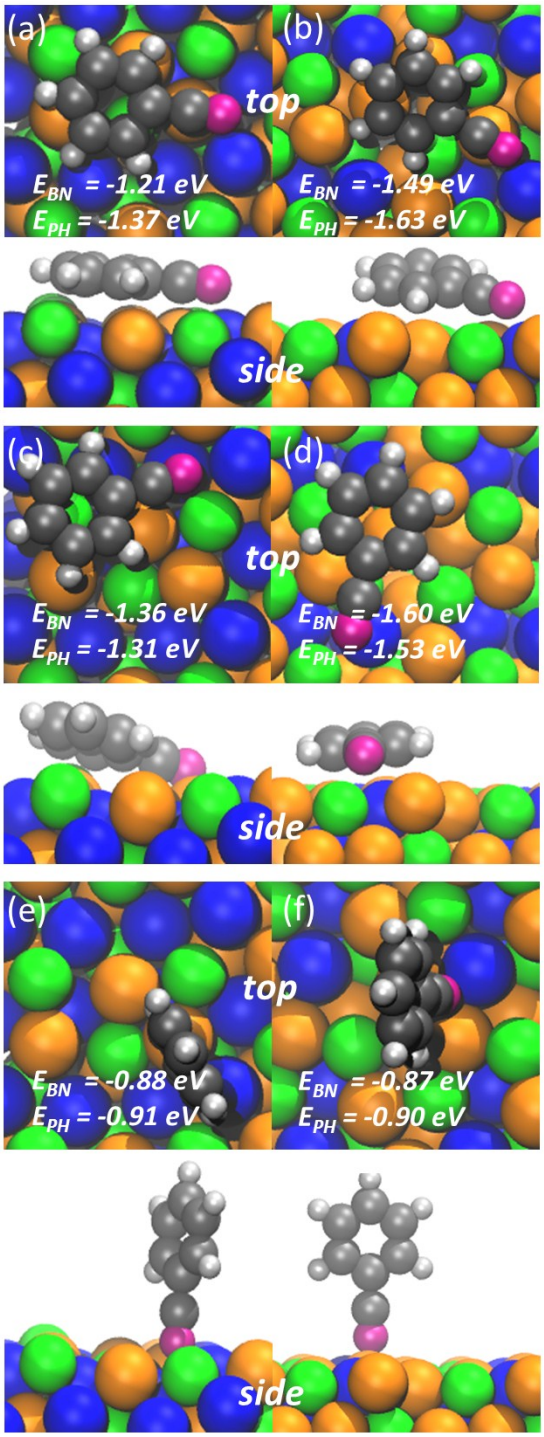

Fig. S4 Adsorption of benzonitrile on the (112) facets for Fe_1Mo_1P (a, c, and e) and $Fe_{1.5}Mo_{0.5}P$ (b, d, and f) with three different binding configurations (a and b; c and d; e and f). E_{BN} and E_{PH} indicate adsorption energies of benzonitrile and phenol under identical binding configurations (orange for Fe; blue for Mo; green for P; grey for C; silver for H; red for O).

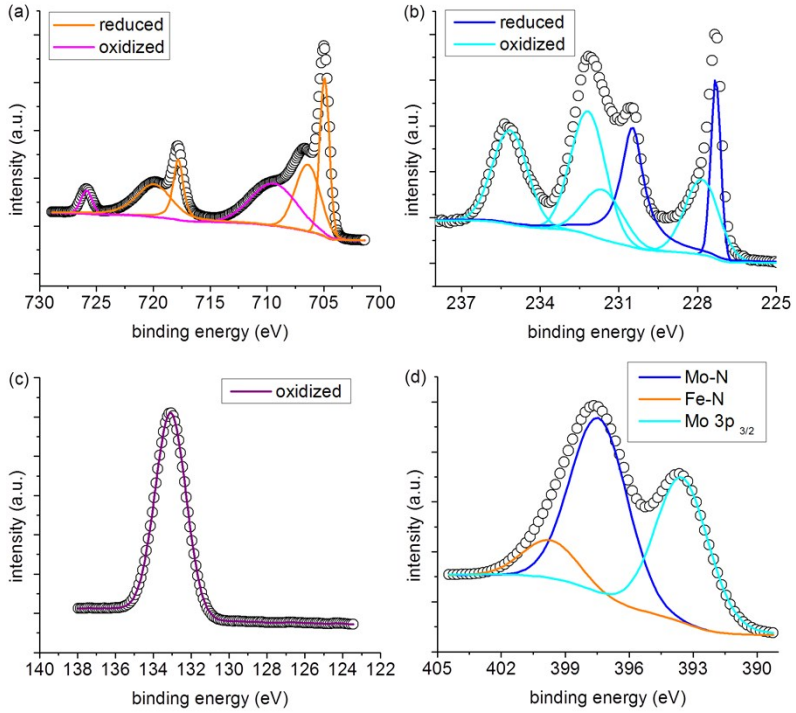

Fig S5 XP spectra of $Fe_{1.55}Mo_{0.45}P$ post TOS run with benzonitrile: (a) Fe 2p, (b) Mo 3d, (c) P 2p, and (d) N 1s and Mo 3p $_{3/2}$ regions. Empty circles and solid lines indicate raw and fitted data, respectively.

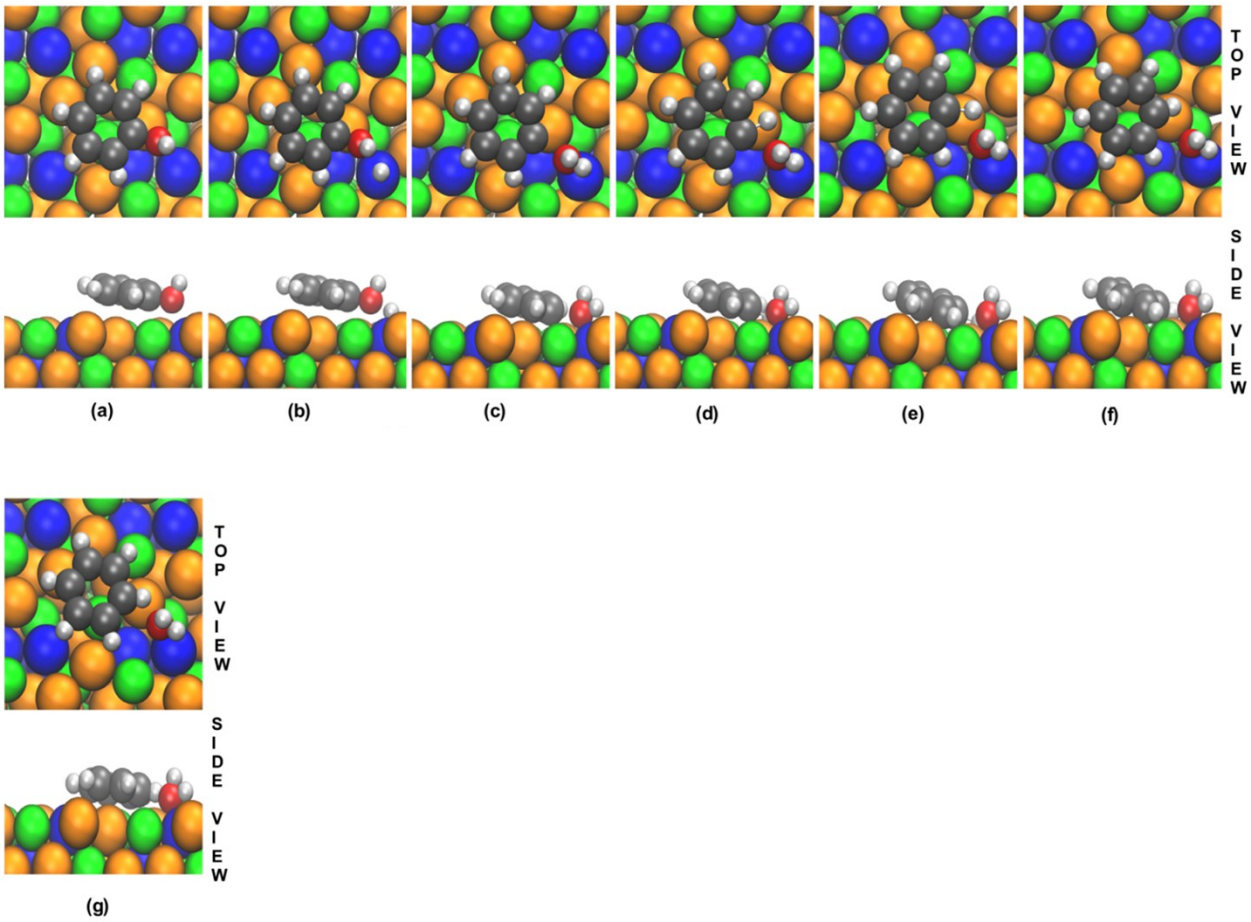

Fig. S6 Optimized structures of phenol (C_6H_5OH), benzene (C_6H_6), and reaction intermediates on (112) facet for $Fe_{1.5}Mo_{0.5}P$ during HDO1: (a) C_6H_5OH*, (b) C_6H_5OH* and H*, (c) C_6H_5-OH_2*(TS), (d) H*, C_6H_5* and OH_2*, (e) H*, rotated C_6H_5*, and H_2O*, (f) C_6H_5-H* and H_2O*, and (g) C_6H_6* and H_2O* (orange for Fe; blue for Mo; green for P; grey for C; silver for H; red for O).

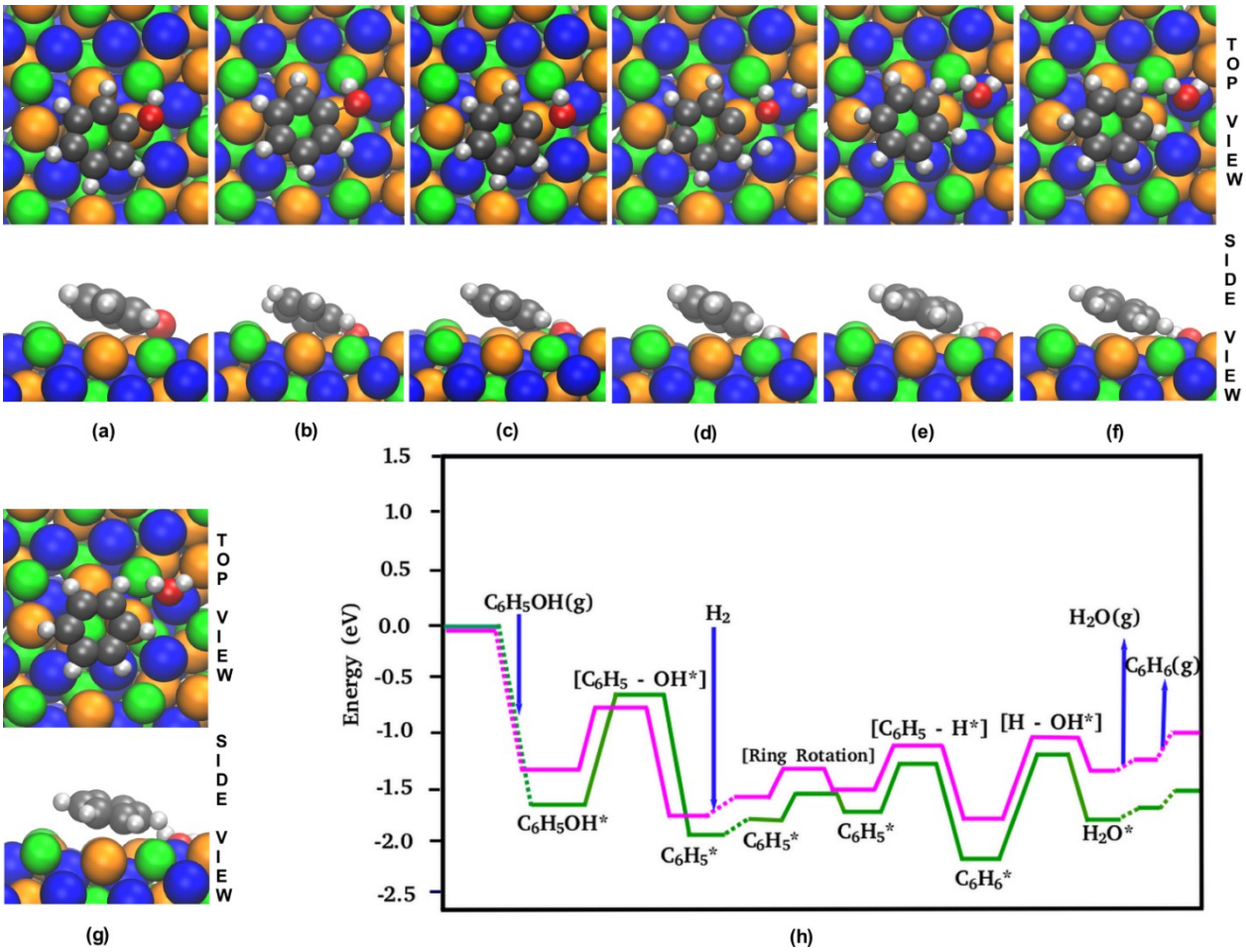

Fig. S7 Optimized structures of phenol (C_6H_5OH), benzene (C_6H_6), and reaction intermediates on the (112) facet for Fe_1Mo_1P during HDO2: (a) C_6H_5OH*, (b) C_6H_5-OH* (transition state (TS)), (c) C_6H_5* and OH*, (d) C_6H_5*, H*, and OH*, (e) H*, rotated C_6H_5*, and OH*, (f) C_6H_5-H* and H-OH*, and (g) C_6H_6* and H_2O* (orange for Fe; blue for Mo; green for P; grey for C; silver for H; red for O). (h) reaction energetics on the (112) facet for Fe_1Mo_1P (magenta) and $Fe_{1.5}Mo_{0.5}P$ (green) during HDO2.

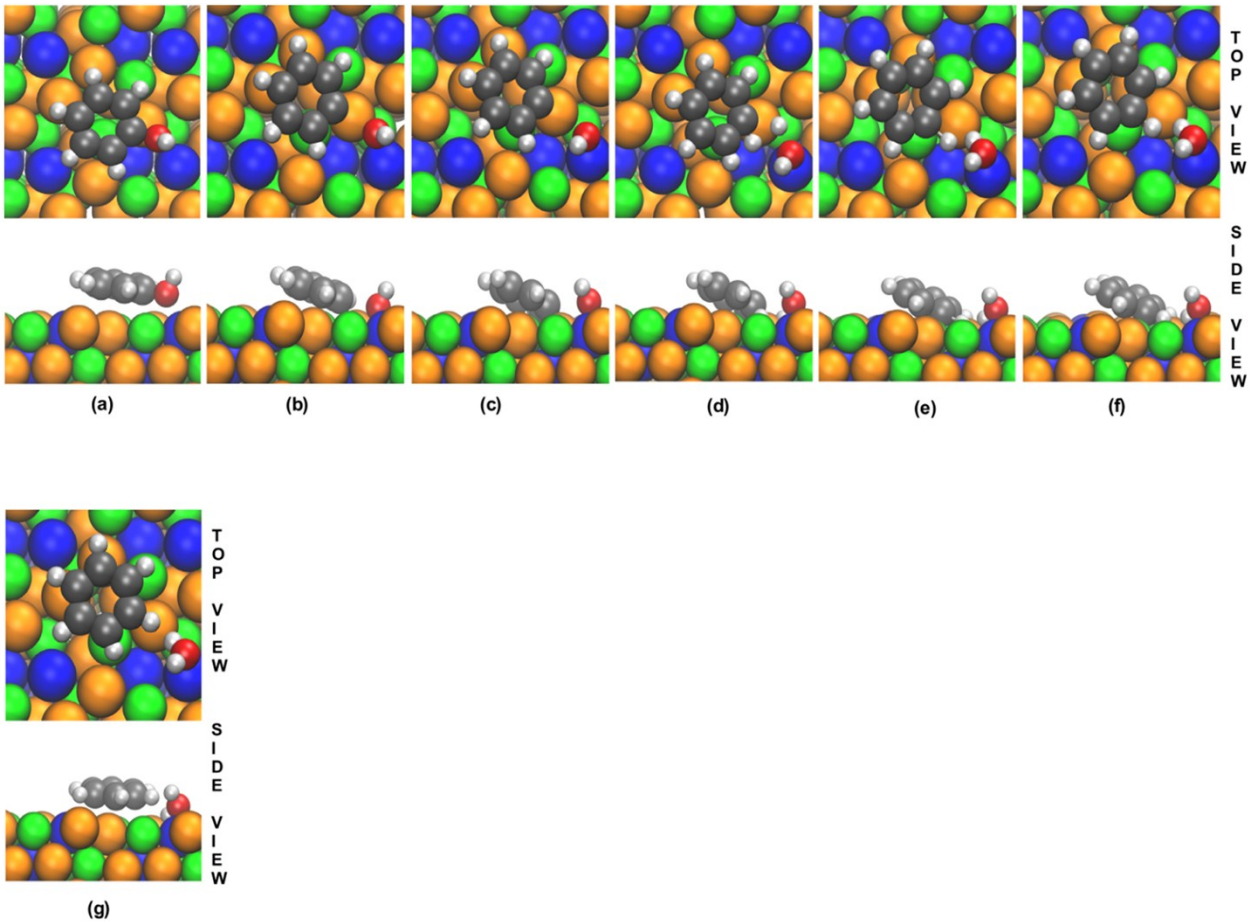

Fig. S8 Optimized structures of phenol (C_6H_5OH), benzene (C_6H_6), and reaction intermediates on (112) facet for $Fe_{1.5}Mo_{0.5}P$ during HDO2: (a) C_6H_5OH*, (b) C_6H_5-OH* (transition state (TS)), (c) C_6H_5* and OH*, (d) C_6H_5*, H*, and OH*, (e) H*, rotated C_6H_5*, and OH*, (f) C_6H_5-H* and H-OH*, and (g) C_6H_6* and H_2O* (orange for Fe; blue for Mo; green for P; grey for C; silver for H; red for O).

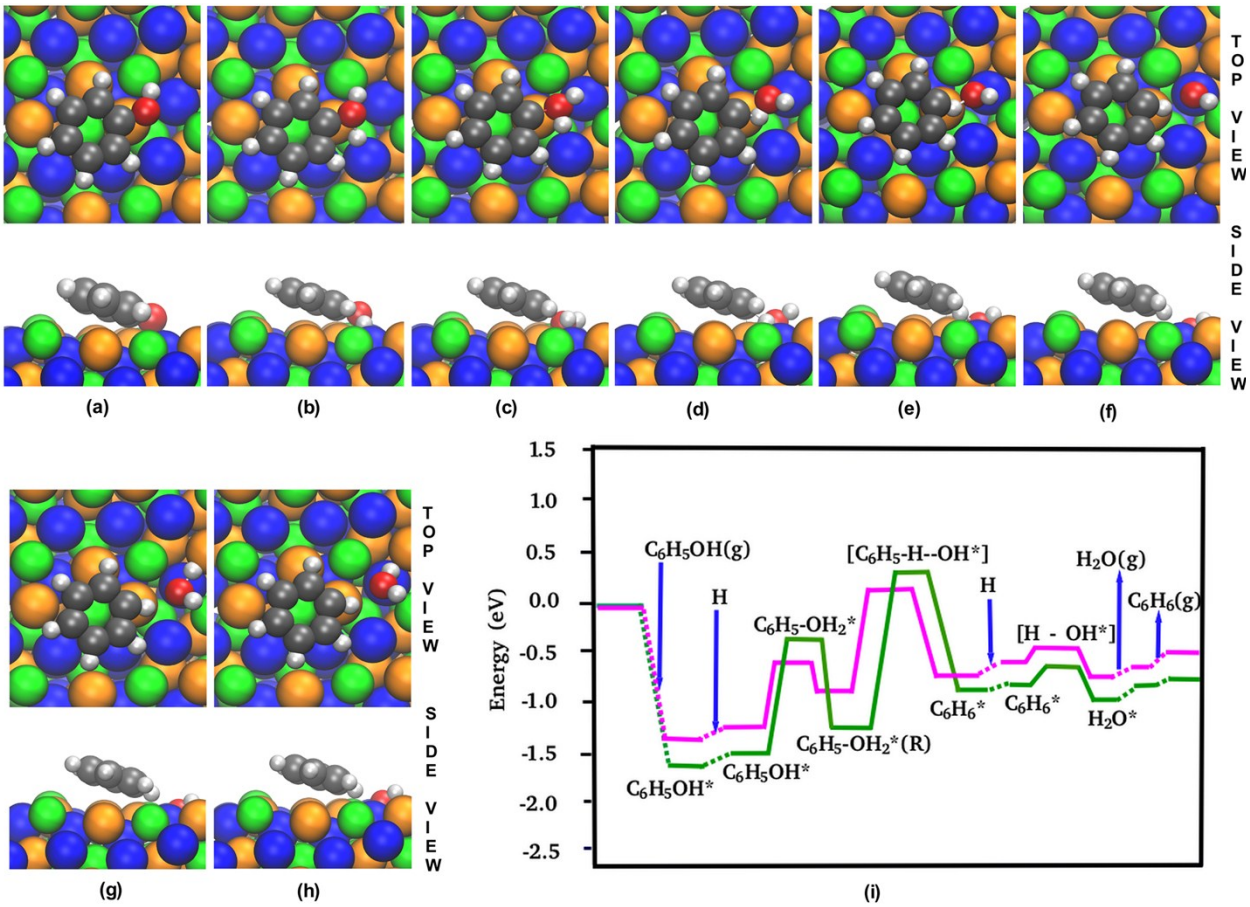

Fig. S9 Optimized structures of phenol (C_6H_5OH), benzene (C_6H_6), and reaction intermediates on (112) facet for Fe_1Mo_1P during HDO3: (a) C_6H_5OH*, (b) C_6H_5OH* and H*, (c) C_6H_5-OH_2*, (d) C_6H_5-OH_2* with rotated hydroxyl group, (e) C_6H_5-H-OH* (TS), (f) C_6H_6* and OH*, (g) C_6H_6*, OH*, and H*, and (h) C_6H_6* and H_2O* (orange for Fe; blue for Mo; green for P; grey for C; silver for H; red for O). (i) reaction energetics on the (112) facet for Fe_1Mo_1P (magenta) and $Fe_{1.5}Mo_{0.5}P$ (green) during HDO3.

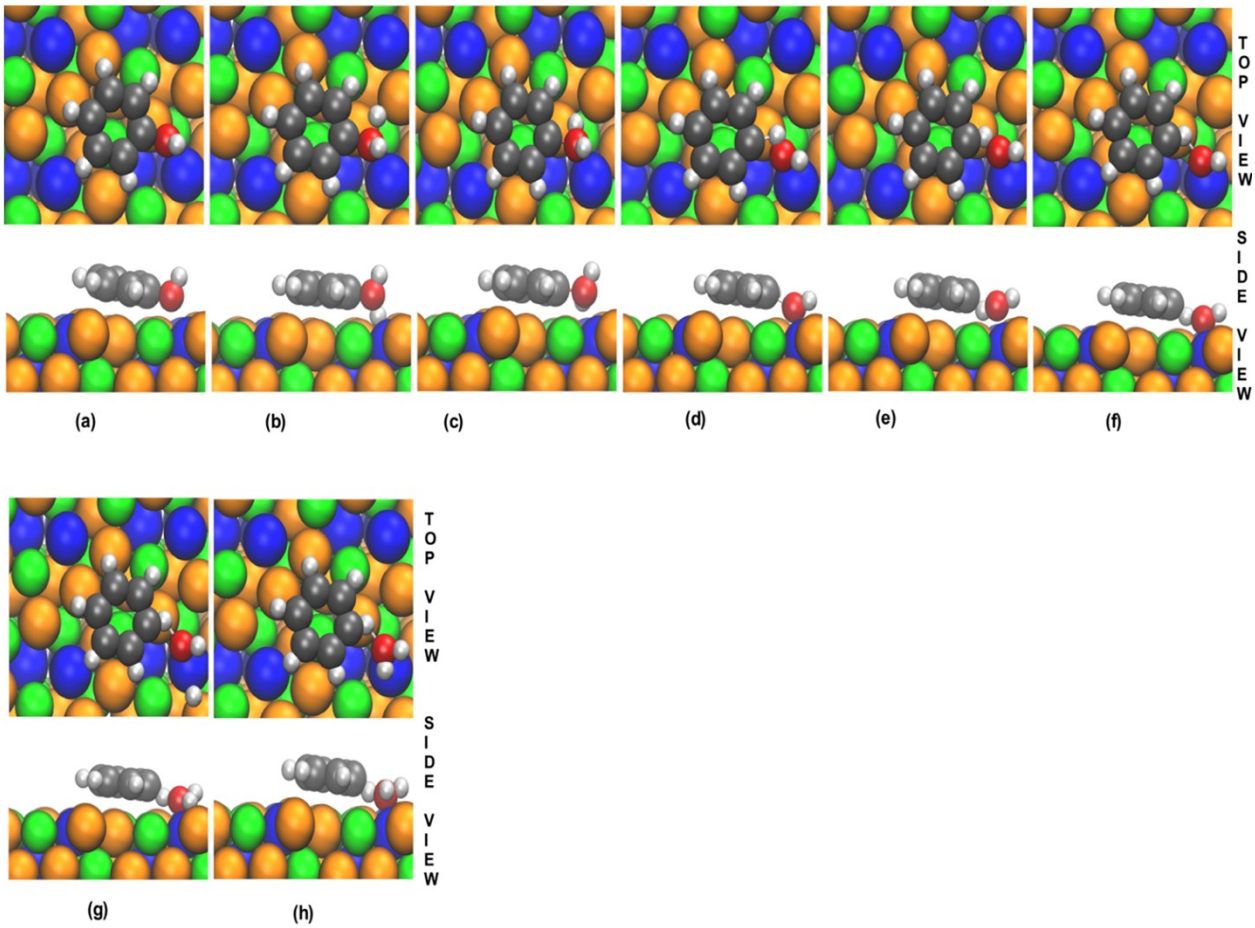

Fig. S10 Optimized structures of phenol (C_6H_5OH), benzene (C_6H_6), and reaction intermediates on (112) facet for $Fe_{1.5}Mo_{0.5}P$ during HDO3: (a) C_6H_5OH*, (b) C_6H_5OH* and H*, (c) C_6H_5-OH_2*, (d) C_6H_5-OH_2* with rotated hydroxyl group, (e) C_6H_5-H-OH* (TS), (f) C_6H_6* and OH*, (g) C_6H_6*, OH*, and H*, and (h) C_6H_6* and H_2O* (orange for Fe; blue for Mo; green for P; grey for C; silver for H; red for O).

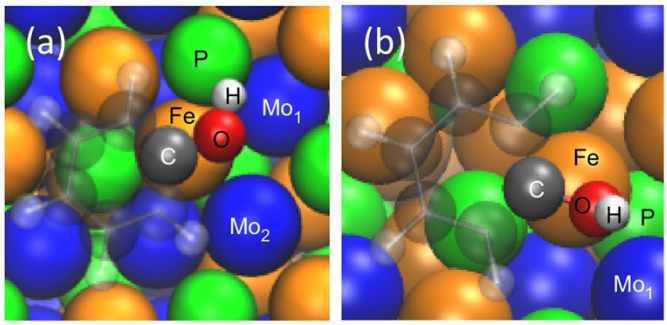

Fig. S11 Atoms on the (112) facets for (a) Fe_1Mo_1P and $Fe_{1.5}Mo_{0.5}P$.

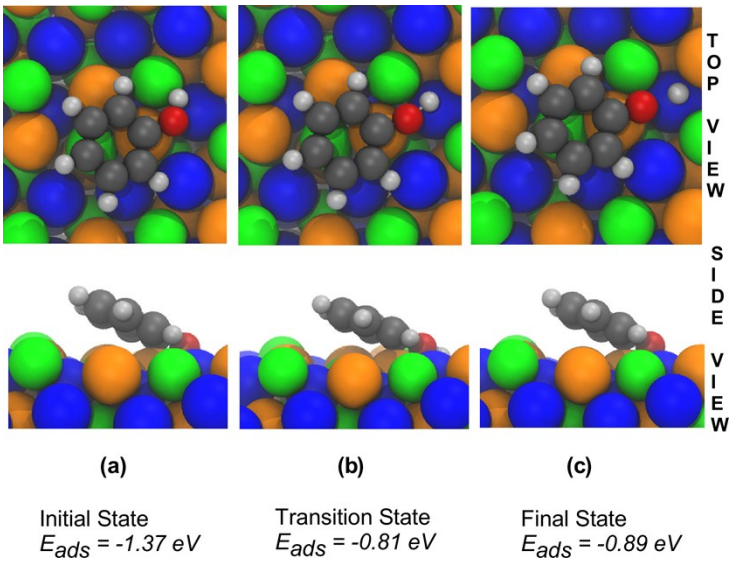

Fig. S12 Deprotonation of phenol on (112) facet for Fe_1Mo_1P: (a) C_6H_5OH*, (b) C_6H_5O-H* (transition state (TS)), and (c) C_6H_5O* and H*. Activation energies required for (a) → (c) and (c) → (a) are 0.56 eV and 0.08 eV, respectively.

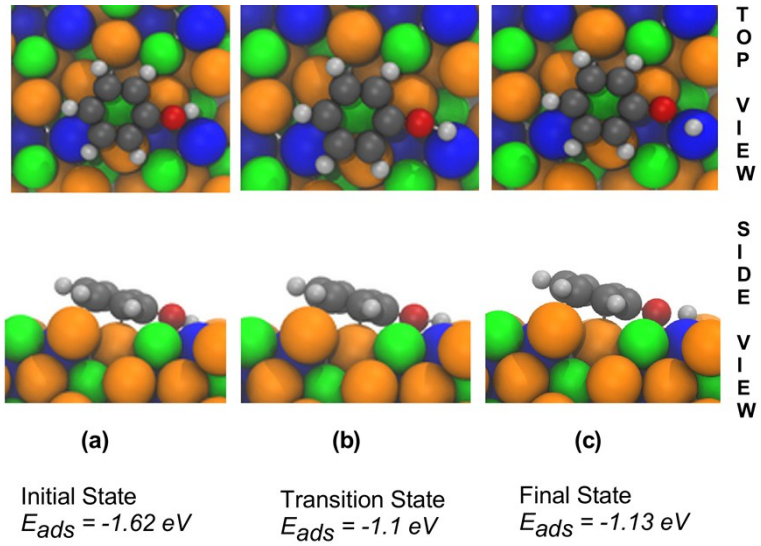

Fig. S13 Deprotonation of phenol on (112) facet for $Fe_{1.5}Mo_{0.5}P$: (a) C_6H_5OH*, (b) C_6H_5O-H* (transition state (TS)), and (c) C_6H_5O* and H*. Activation energies required for (a) → (c) and (c) → (a) are 0.52 eV and 0.03 eV, respectively.